

OPEN ACCESS

Polyvinylidene Difluoride–Polyethyleneoxide Blends for Electrospun Separators in Li-Ion Batteries

To cite this article: A. La Monaca *et al* 2017 *J. Electrochem. Soc.* **164** A6431

View the [article online](#) for updates and enhancements.

You may also like

- [Boosting the electro-mechanical coupling of piezoelectric polyvinyl alcohol–polyvinylidene fluoride blends by dispersing nano-graphene platelets](#)
Dimitra Valadorou, Anthony N Papathanassiou, Eirini Kolonelou et al.
- [Poly\(vinylidene fluoride\)-Based Al Ion Conductive Solid Polymer Electrolyte for Al Battery](#)
Masashi Kotobuki, Li Lu, Seruguei V. Savilov et al.
- [Thermally Stable Gel Polymer Electrolytes](#)
Min-Kyu Song, Young-Taek Kim, Yong Tae Kim et al.



Your Lab in a Box!

The PAT-Tester-i-16: All you need for Battery Material Testing.

- ✓ All-in-One Solution with integrated Temperature Chamber!
- ✓ Cableless Connection for Battery Test Cells!
- ✓ Fully featured Multichannel Potentiostat / Galvanostat / EIS!

www.el-cell.com +49 40 79012-734 sales@el-cell.com


electrochemical test equipment





FOCUS ISSUE OF SELECTED PAPERS FROM IMLB 2016 WITH INVITED PAPERS CELEBRATING 25 YEARS OF LITHIUM ION BATTERIES

Polyvinylidene Difluoride–Polyethyleneoxide Blends for Electrospun Separators in Li-Ion Batteries

A. La Monaca,^a F. De Giorgio,^a M. L. Focarete,^a D. Fabiani,^b M. Zaccaria,^b and C. Arbizzani^{a,*}

^aDepartment of Chemistry “Giacomo Ciamician”, Alma Mater Studiorum - Università di Bologna, Bologna, Italy

^bDepartment of Electric, Electronic and Information Engineering “Guglielmo Marconi”, Alma Mater Studiorum - Università di Bologna, Bologna, Italy

Polyvinylidenedifluoride (PVdF) and polyethyleneoxide (PEO) are blended and electrospun in order to obtain membranes suitable as Li-ion battery separators. The separators are characterized, and their properties investigated and compared with those of PVdF and commercial separators. The PVdF-PEO based separators ensure increased conductivities, greater electrolyte uptake and higher porosities than commercial polyolefines, all factors that improve cell performance. They are also safer than PVdF separators thanks to lower shutdown temperature, even if their mechanical properties are not yet comparable with those of the latter.

© The Author(s) 2017. Published by ECS. This is an open access article distributed under the terms of the Creative Commons Attribution 4.0 License (CC BY, <http://creativecommons.org/licenses/by/4.0/>), which permits unrestricted reuse of the work in any medium, provided the original work is properly cited. [DOI: 10.1149/2.0651701jes] All rights reserved.



Manuscript submitted September 7, 2016; revised manuscript received January 13, 2017. Published February 2, 2017. This was Paper 269 presented at the Chicago, Illinois, Meeting of the IMLB, June 19–24, 2016. *This paper is part of the Focus Issue of Selected Papers from IMLB 2016 with Invited Papers Celebrating 25 Years of Lithium Ion Batteries.*

Li-ion batteries are one of the most mature and most wide spread energy storage systems on the market. They supply almost every laptop, smartphone and tablet and are among the most widely used storage systems in hybrid and electric vehicles. Today Li-ion technology is approaching its limits of energy density (200–250 Wh/kg)^{1,2} thanks to new and advanced high-voltage and high-capacity electrode materials. Hence, most electrochemical research seeks to improve cycle life and safety.^{2–9} However, in order to meet the new conditions required by high voltage electrodes and to enhance the other aforementioned features, the development of so-called inactive materials is mandatory. A key inactive material is the separator. It prevents physical and electrical contact between electrodes while allowing ions to flow through it. It must have a high chemical and electrochemical stability vis-à-vis the electrode and electrolyte materials and should be mechanically strong enough to withstand the high stress during battery assembly. The separator must also be sufficiently porous to absorb a large quantity of liquid electrolyte, thus assuring high ionic conductivity. On the other hand, the separator inevitably increases the electrical resistance of the cell, thereby significantly worsening the battery performance. Indeed, it must be very thin and porous in order to achieve high energy and power densities while ensuring sufficient mechanical robustness.^{10–13} The perfect separator has yet to be invented, its development depending on trade-offs among the aforementioned properties in order to obtain the specific features for the desired application. Safety too is an important concern. A necessary feature of separators is the shutdown function, i.e. the ability to shut the battery down when overheating occurs due, for example, to a short circuit, overcharging or exposure to external heat sources, in order to prevent thermal runaway.^{14,15} Nearly all separators today used in liquid electrolyte batteries are based on microporous polyolefin membranes given their good mechanical properties, thinness and low cost. Much research effort of late has been devoted to the development of innovative, highly porous separators based on non-woven mats. One well known method of mat preparation is electrospinning technology.^{13,16,17} Electrospinning is a low cost technology with respect to other techniques used to manufacture nanofibers, e.g. extrusion, drawing, phase separation. It is also commonly used to fabricate highly porous nanostructures or nanofibrous non-woven membranes characterized by high open porosity and high surface area which lead to massive electrolyte uptake and, hence, to excellent ionic conductivity.

Several polymers have been electrospun and used as separators.¹⁸ Polyvinylidenedifluoride (PVdF) and its copolymers are probably the most widely studied.^{18–25} PVdF is characterized by excellent electrochemical stability, and its high dielectric constant ($\epsilon = 8.4$) permits better dissolution of lithium salts and, thus, a larger amount of charge carriers. One PVdF drawback is a high melting point that does not execute the shutdown function.^{22,26} We submit a novel strategy to overcome this limitation by blending PVdF with a polymer of lower melting-point such as polyethyleneoxide (PEO), which can also coordinate and transport Li^+ through local relaxation and segmental motion of its chains and improve ionic conductivity. To the best of our knowledge, only two papers have investigated the effect of PEO on ionic conductivity and the electrochemical properties of PVdF-based polymer gel electrolytes. Both report better performance characteristics of PVdF/PEO membranes with respect to PVdF membrane.^{27,28} In the present work blends of PVdF and PEO are electrospun in order to yield separator membranes for Li-ion batteries. The separators are fully characterized, and their properties investigated and compared with those of PVdF and of a polyolefine commercial separator.

Experimental

Materials.—Ultra-high-molecular-weight polyvinylidenedifluoride (PVdF, Solef 6020, M_w 690,000 g mol^{-1}) was provided by Solvay Specialty Polymers. Polyethylene oxide (PEO) of low (M_v 100,000 g mol^{-1}) and high (M_v 1,000,000 g mol^{-1}) molecular weight and N,N-Dimethylformamide (DMF) were purchased from Sigma-Aldrich and used as received. A commercial Celgard2400 separator (Celgard) was used for comparative analyses. A solution of 1 M LiPF_6 in ethylene carbonate (EC):dimethyl carbonate (DMC) (1:1 w/w) (LP30 Selecti-Lyte, Merck KGaA, 20 ppm H_2O) was used for electrolyte uptake and electrochemical tests.

Electrospun membrane preparation.—Two blends of PVdF:PEO with a 90:10 w/w composition were prepared using PEO with low and high molecular weight, hereinafter called B100 and B1000, respectively. A careful screening of working conditions has been made in order to obtain mats composed of fibers without beads and with good mechanical properties. Each system was optimized individually, slightly changing the total polymer concentration in order to achieve the best fiber morphology. We used a concentration of 15% w/v for B100 solution to obtain beads-free fibers. The electrospinning of B1000 solution at the same concentration was impossible

*Electrochemical Society Member.

^zE-mail: catia.arbizzani@unibo.it

because the blend behaved like a solid, jelly-like material. Hence, B1000 concentration was lowered to 10% w/v. PVdF and PEO were first dissolved in DMF at optimized total polymer concentrations of 15% and 10% w/v for B100 and B1000, respectively. A mild heating (~10 min at 40°C) was set to help the dissolution process during overnight stirring with a magnetic hot plate stirrer. The electrospinning apparatus was composed of a syringe pump (KDSscientific), a glass syringe, a stainless-steel, blunt-ended needle (inner diameter = 0.5 mm) connected to a high voltage power supply (Spellman, SL 50 P 10/CE/230) and a grounded cylindrical rotating collector (length = 12 cm, diameter = 5 cm, rotation angular speed = 50 rpm). The polymer solution was dispensed from the needle, fixed to a support rod and placed 22 cm apart from the collector.²⁹ The electrospinning process was carried out in a glove box at room temperature (RT) and relative humidity of 40–45% with a solution flow-rate of 0.4 mL/h and 20 kV applied voltage. Membranes with thickness in the range of 40–100 μm were obtained. A PVdF membrane was also prepared for comparison by dissolving the polymer in DMF at a concentration of 16% w/v. Electrospinning parameters were the same used for B100 and B1000 except for the flow rate that was 0.3 mL/h.

Circular electrospun polymer separators (EPSs) of 0.785 cm² geometric area were then cut from the membranes by a puncher. Some separators were pressed with a hydraulic E-Z Press (ICL) at 500 psi for 15 min at RT in order to improve dimensional stability, especially after electrolyte uptake. The pressed EPSs are indicated as PVdFp, B100p and B1000p.

All the EPSs were dried at 80°C under vacuum for 4 h in a Büchi B-585 Kugelrohr in order to remove any trace of residual solvent and humidity and transferred in an argon filled MBraun Labmaster SP dry box (< 0.1 ppm H₂O, < 0.1 ppm O₂) for use.

Characterization.—Fiber morphology was investigated using a Philips 515 Scanning electron microscope (SEM) at an accelerating voltage of 15 kV; the samples were sputter-coated with gold before SEM analysis. Wide-angle X-ray diffraction measurements (WAXD) were performed at RT with a PANalytical X'Pert PRO diffractometer equipped with an XCelerator detector. X-ray diffraction data were collected in the 2θ range of 5°–60° using CuK radiation (λ = 0.15418 nm) as X-ray source. Thermogravimetric analysis (TGA) was carried out using a TA Instruments TGA2950 analyzer from RT to 600°C with a heating rate of 10°C/min in nitrogen atmosphere. Differential scanning calorimetry (DSC) measurements were performed using a TA Instruments Q100 equipped with the Liquid Nitrogen Cooling System (LNCS) accessory. DSC measurements were carried out in helium atmosphere from –100°C to 250°C with a heating scan rate of 20°C/min. From the DSC thermograms, the glass transition temperature (T_g) was taken at half-height of the glass transition heat capacity step, and the melting temperature (T_m) was taken at peak maximum of the melting endotherm. Tensile tests were carried out with an Instron 4465 machine, applying a cross-head speed of 2 mm/min. Tests were performed on a specimen 50 mm long and 5 mm wide, with a gauge length of 20 mm. Ten specimens per mat were tested and the results processed through Weibull probability distribution, which provides the 63.2th percentile (α) with the confidence intervals at 90% probability. Stress-at-break (σ_b), elongation-at-break (ε_b) and Young's elastic modulus were then obtained. The electrolyte uptake of the EPSs was evaluated by soaking them in LP30 for 2 h inside the dry box and then removing excess electrolyte with filter paper. The uptake was calculated by Equation 1

$$U(\%) = (W_w - W_d)/W_d \times 100 \quad [1]$$

where W_w and W_d are the wet and dry membrane weights, respectively.

Resistivity of the electrolyte-soaked membranes was measured by electrochemical impedance spectroscopy (EIS) using a Solartron SI 1255 frequency response analyzer coupled with an EG&G Model 273A PAR potentiostat/galvanostat. For EIS analysis, a T-shaped Teflon cell (BOLA by Bohlender GmbH) was assembled with the soaked EPS interposed between stainless steel (SS) blocking elec-

trodes (0.785 cm²) in symmetrical configuration SS/EPS/SS. The cell was placed in a Memmert IPP 200 incubator at 30°C and the measurements were performed after one hour in order to let the system stabilize. EIS measurements were carried out by applying an AC perturbation of 5 mV with a variable frequency from 100 kHz to 1 Hz, collecting 10 points per decade. MacMullin numbers were calculated from resistivity values by Equation 2

$$N_m = \frac{\rho_s}{\rho_e} \quad [2]$$

where ρ_s is the resistivity of the soaked separator and ρ_e the resistivity of the electrolyte after Schmidt et al.³⁰

EIS measurements with blocking electrodes were also exploited to evaluate the shutdown properties of the EPS during an abnormal temperature rise. The cell was placed in a Memmert UNB 100 oven and the temperature raised from 30°C to 200°C; the EIS analyses were performed every 30°C up to 60°C and then every 10°C up to 200°C.

EIS spectra of symmetric Li/Li cells with different separators soaked with LP30 were also carried out at 30°C in open circuit condition from 100 kHz to 100 mHz (5 mV AC, 10 point/decade) to investigate the chemical reactivity of the Li/electrolyte interface over time.

The water content of membranes was evaluated with a Metrohm 831 KF coulometer. The membranes were dried for 2, 4 and 20 hours and placed in LP30 solutions for few minutes. Hence, the water content of the solutions with the membrane inside was measured.

Cell assembly.—For the electrochemical tests in half-cell configuration, the soaked EPS was put in a BOLA cell together with a positive electrode based on LiFePO₄, and a negative electrode of lithium metal (in excess); lithium metal was also used as reference electrode. The positive electrode material was 90 wt% LiFePO₄ (Advanced Lithium Electrochemistry Co. Ltd.), 5 wt% Super P (Erachem) as conductive carbon and 5 wt% PVdF Kynar HSV 900 (Arkema) as binder. The LiFePO₄ electrodes were prepared by dry mixing the three powders and then adding the *N*-methyl pyrrolidone. The slurry was spread with a mini-coating machine (MC 20, Hohsen Corp.) on KOH-etched aluminum foil as current collector. After drying at 80°C overnight, circular electrodes of 0.636 cm² geometric area were cut by puncher, pressed with a hydraulic E-Z Press (ICL) at 3000 psi for 3 minutes and dried overnight at 120°C.

Graphite electrodes (89% Superior graphite, 8% PVdF, 3% pure black) on copper current collectors were used in full cell configuration. The electrochemical tests were performed by a VMP multichannel potentiostat/galvanostat (Bio-logic Science Instruments) at 30°C.

Results and Discussion

In electrospinning several parameters, mainly related to the process, to the ambient conditions and to the solution properties, influence fiber morphology and, hence, porosity, thickness, mechanical and physical characteristics of the resulting separators. It is well known that polymer concentration and molecular weight play an important role in fiber formation. Usually, beads-free nanofibers and increased fiber diameters are obtained by increasing polymer concentration and molecular weight.³¹ Electrospinning conditions were optimized specifically for each of the three polymeric solutions, i.e. B100, B1000, PVdF, in order to obtain membranes composed of regular bead-free fibers with comparable sub-micrometric diameters, as shown in the SEM images of Figures 1a–1f. Thanks to the high molecular weight of PEO1000, a concentration of 10% w/v was sufficient to obtain a solution with a viscosity appropriate for electrospinning. By contrast, a higher concentration (16% w/v for PVdF and 15% w/v for B100) was necessary for the other two solutions. Indeed, solution viscosity, which is governed by polymer molecular weight and concentration, is known to be the key parameter for obtaining bead-free continuous fibers.³² The non-woven mats were composed of multi-layered, three-dimensional network structures. The B100 membrane was composed of fibers having a broader distribution of diameters,

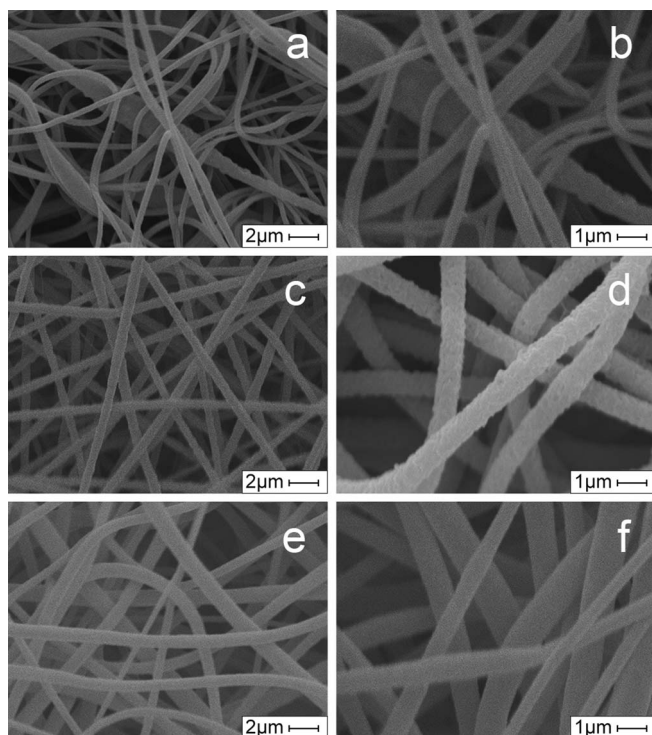


Figure 1. SEM images of (a, b) B100, (c, d) B1000 and (e, f) PVdF.

varying in the 300–800 nm range (Figure 1a), the B1000 membrane (Figure 1c) was characterized by a homogeneous distribution of fiber diameters (~800 nm); the PVdF membrane showed fibers with diameters in the range 500–1000 nm (Figure 1e). The trend toward low thickness is consistent with the lower average molecular weight of the polymer blend B100 than PVdF and B1000. The rough surface of the blended fibers is also notable in the high magnification images (Figures 1b and 1d) and contrasts with the smooth surface of PVdF fibers (Figure 1f). This feature was already been reported^{27,28} and may be associated with the hygroscopic nature of PEO, which is responsible for moisture absorption during fiber formation. This particular surface roughness is connected to the fiber porosity, which is beneficial for wettability and, accordingly, for the separator's electrolyte uptake.

The electrospun polymer separators (EPSs) were made to a greater thickness (40–100 μm) than that of commercial separators based on polyolefinic film (20–25 μm). Given the very high porosity of the electrospun non-woven mats, a thickness near 40 μm assures good mechanical properties without affecting the electrochemical performance of the cell.³³

WAXD measurements were performed in order to investigate the molecular structure and crystalline phases of the membranes and the related diffractograms are shown in Figure 2.

Five crystal phases (α , β , γ , δ , and ϵ) are reported for PVdF.³⁴ While some give reflections at very similar diffraction angles, each phase has one or two characteristic peaks that allow their identification. During electrospinning, the polymeric solution is subjected to two main forces: shear when it flows inside the needle and a coulomb force when the jet is elongationally stretched between the needle and the collector by the high electric field. These two forces lead to disentanglement and subsequent parallel arrangement of the macromolecular chains.³⁵

Therefore, the formation of a large quantity of β phase can be achieved.^{36,37} This phase can be identified in all specimens in correspondence to the following peaks: $2\theta = 20.6^\circ$ associated to the sum of (110) and (200) crystal planes diffractions, 36.2° related to (201) plane, and 41.1° corresponding to (111) diffraction. The peaks at around $2\theta = 18.4^\circ$ (020), 20° (110) and 26.5° (021) belong to the α

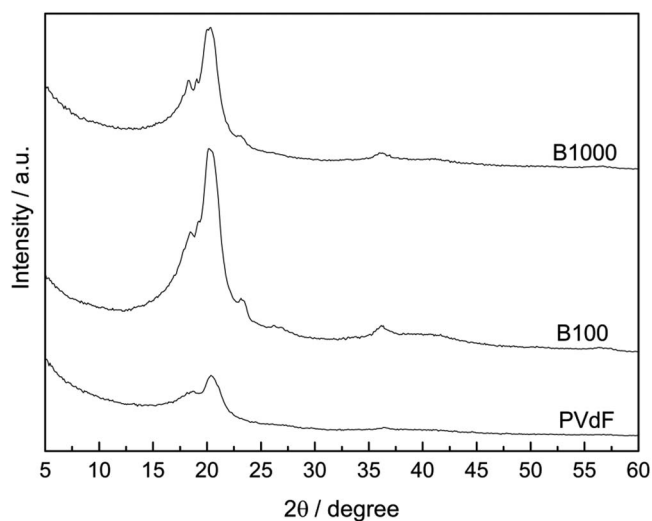


Figure 2. WAXD spectra of PVdF, B100 and B1000 membranes.

phase of PVdF. Therefore, in all three EPSs, α and β phases coexist.³⁴ Moreover, Martins et al.²⁶ proved that it is nearly impossible to discern between γ and α phase of PVdF by means of X-ray diffractions due to the similar peak positions of the two phases. Hence, the presence of the γ phase in the tested samples cannot be excluded. The characteristic PEO peaks can be detected at around $2\theta = 19^\circ$ (120) and 23.4° (112) in the B100 and B1000 diffractograms. As expected, these peaks are weak in intensity, due to the low amount of PEO (10 wt%) in the blends.

The thermal stability of B100 and B1000 was investigated through TGA measurements and compared to that of the relative homopolymers. The thermograms of the two blends displayed in Figures 3a and 3b show a characteristic two-step curve: the first weight loss step corresponds to the thermal degradation of PEO and the second to that of PVdF. The magnitude of each weight loss step correlates well with the amount of each component in the blend.

The TGA curves show a carbonaceous residue above 500°C, mainly due to degradation of PVdF in N_2 atmosphere. As suggested by Botelho et al.³⁷ the scission of C-H and C-F bonds starts in the first step of thermal degradation of PVdF and leads to the formation of HF. The subsequent loss of HF leads to the formation of polyenic sequences inside the polymeric chain. The instability of these sequences brings about consecutive degradation steps, which produce aromatic molecules and then polyaromatic chains that are indecomposable in inert atmosphere.

DSC thermograms of B100 and B1000 were compared with the curves of the plain homopolymers (Figures 4a and 4b). Two melting endotherms are evident in the thermograms of B100 and B1000: the first at $T_m = 61^\circ\text{C}$ (B100) - 64°C (B1000) and the second at $T_m = 168^\circ\text{C}$ (B100) - 166°C (B1000) correspond to the melting point of PEO100 homopolymer ($T_m = 64^\circ\text{C}$), PEO1000 homopolymer ($T_m = 69^\circ\text{C}$) and PVdF homopolymer ($T_m = 168^\circ\text{C}$), respectively. This indicates that during electrospinning the two polymers are phase-separated, as reported elsewhere.²⁷

Even though PEO and PVdF chains are tangled together inside the fibers, their crystallization processes are totally independent and occur without any hindrance or co-crystallization. The small shift in melting temperature of PVdF and PEO components in the blends, compared to homopolymers, may be attributed to the interactions of ether oxygen of PEO and fluoride of PVdF. These shifts are more evident in the B1000 DSC curve, probably because the longer PEO1000 chains increase the number of interactions with PVdF.

Figure 5 shows elastic modulus, stress at break and elongation at break of the two blended membranes. They show similar mechanical performance, as expected considering the same ratio of the two homopolymer inside the blends. Note the evident difference

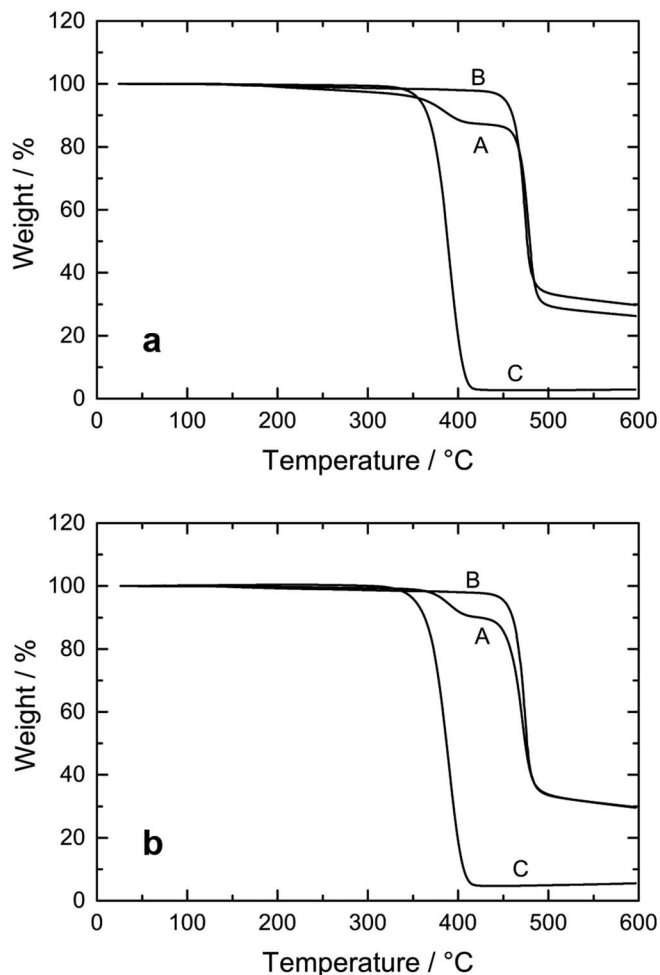


Figure 3. (a) Thermogravimetric curves of B100 (A) and of its components, PVdF (B) and PEO100 (C). (b) Thermogravimetric curves of B1000 (A) and of its components, PVdF (B) and PEO1000 (C).

between the stress-at-break values of B100 and B1000: the former is nearly three-fold higher than the latter, and the gap can be attributed to the different morphology of the membranes. As shown and discussed for Figure 1, the membrane fibers exhibit different diameters, B100 having lower and more broadly distributed diameters (300–800 nm) than B1000 (~800 nm). This could be related to the different PEO molecular weight, as reported in literature for polystyrene and polyvinylalcohol.^{31,38,39} Richard-Lacroix et al.³⁸ demonstrated that reducing fiber diameter toward the nanoscale leads to an increasingly high level of orientation of the macromolecular chains of atactic polystyrene, inside the fiber and to an increasing apparent level of disentanglement of the chains. Thus, a more evident alignment occurs inside a thinner fiber, conferring higher mechanical performance on the material. The correlation between fiber diameter and mechanical properties was proven by Gao et al. for electrospun PVdF membrane.⁴⁰ They observed that reducing the average fiber diameter from 884 nm to 514 nm involved an increase of tensile modulus (from 95 MPa to 117 MPa) and of maximum stress (from 5.3 MPa to 6.5 MPa) and a decrease of elongation (from 19.51% to 15.65%). Thus, our data for B100 and B1000 are consistent with those in literature for plain PVdF membranes.^{21,28,40,41}

A first step toward upgrading the mechanical performance of electrospun membranes is further optimization of the electrospinning process in order to narrow and homogenize the fiber diameters. Further improvements entail the incorporation of inorganic oxide nanoparticles in the polymeric fibers during electrospinning³³ and the exposure of the polymeric solution to a plasma jet for a few minutes before

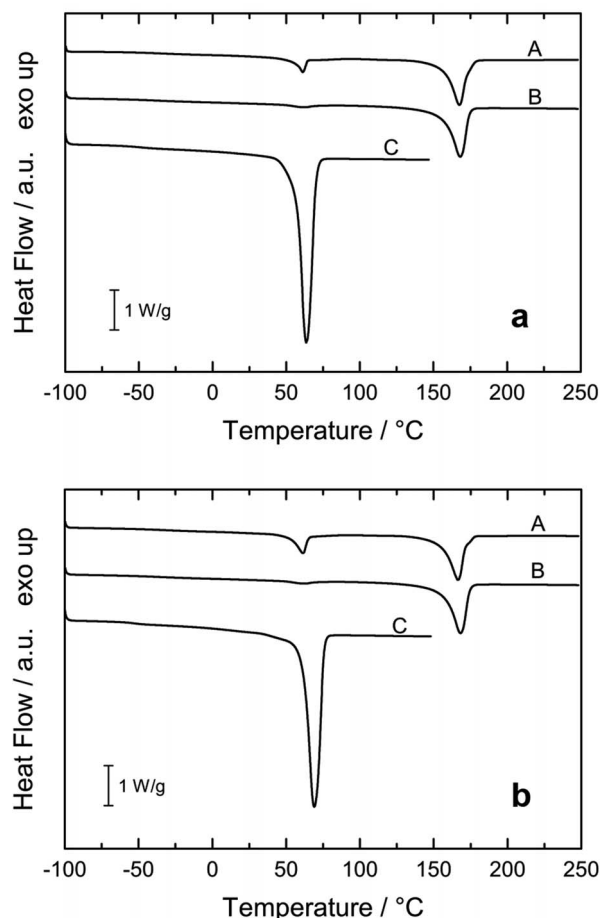


Figure 4. (a) DSC analysis of B100 (A), PVdF (B) and PEO100 (C). (b) DSC analysis of B1000 (A), PVdF (B) and PEO1000 (C).

electrospinning, which was found to improve both stress-at-break and elongation-at-break.⁴²

The electrolyte uptake values of PVdF, B100 and B1000 at RT are shown in Table I. The uptake is improved by the presence of PEO100 in the blend. The weight increase of B100 is the highest, probably due to the enhanced mobility of shorter PEO100 chains. By contrast, the electrolyte uptake value obtained for B1000 is slightly lower than

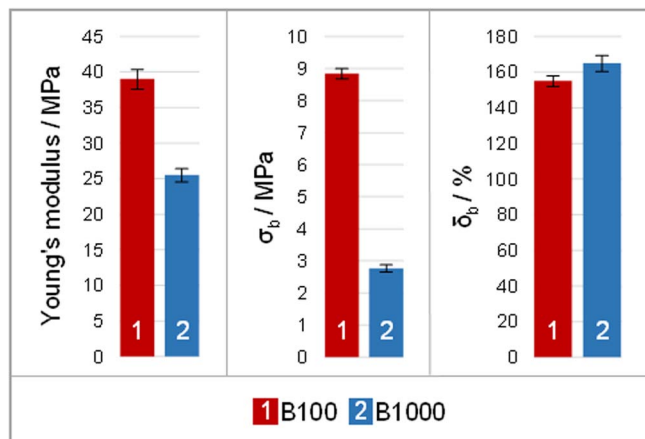


Figure 5. Mechanical properties of B100 and B1000: Young's modulus (left), stress at break – (σ_b , center) and elongation at break (δ_b , right).

Table I. Electrolyte uptake of pristine and pressed membranes.

Separator	Electrolyte Uptake
PVdF	440%
B100	527%
B1000	303%
PVdFp	81%
B100p	84%
B1000p	58%
Celgard2400	100%

that of PVdF, although the values of all three membranes were much higher than that of Celgard2400.

As noted *supra*, EPS becomes difficult to handle when wetted by the electrolyte due to its gel-like nature when soaked. In order to enhance its dimensional stability, some separators from the three membranes were pressed. The macroscopic aspect of the pressed membranes is comparable; the pressed membrane B1000p is shown in Figure 6a, as an example, together with the pristine B1000 for comparison. Pressing considerably decreases porosity, as shown by the SEM images (Figure 6). The PVdFp membrane seems to be especially affected by pressing (Figure 6b). By contrast, B100p and B1000p show areas of differing, i.e. non-uniform, porosity (Figures 6c and 6d).

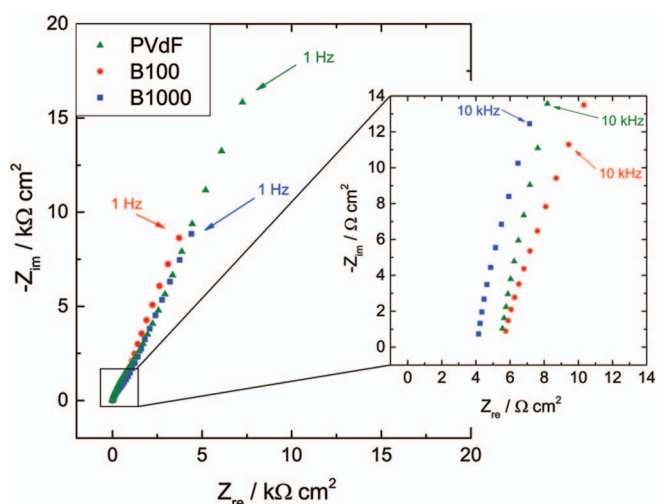
Electrolyte uptake was also performed on the pressed EPSs (Table I). As expected, the results show lower values than those of the pristine but comparable to those of Celgard2400 uptake. This response deserves further investigation, especially concerning the evaluation of pressing conditions in terms of pressure values and processing time.

The enhanced porosity and higher electrolyte uptake of pristine EPSs are expected to increase ionic conductivity, thereby decreasing the contribution of the separator to cell internal resistance. This can result in better battery performance at high currents. EIS measurements were thus performed in order to evaluate resistivity and MacMullin number of the separators. It is necessary to calculate MacMullin numbers, as shown in Table II, to compare separators of different thickness. Figure 7 shows the Nyquist plots of the pristine EPSs. As can be seen, the lowest value was obtained with B1000, the less resistive separator among the tested ones. Even B100, the most resistive, yielded a MacMullin number lower than that of Celgard2400.^{43,44}

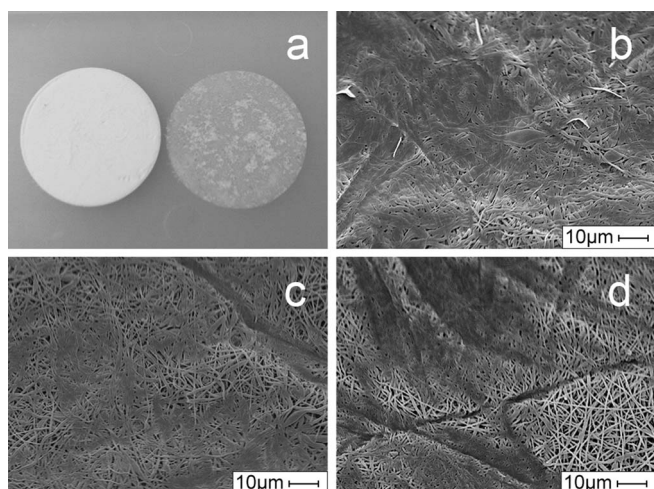
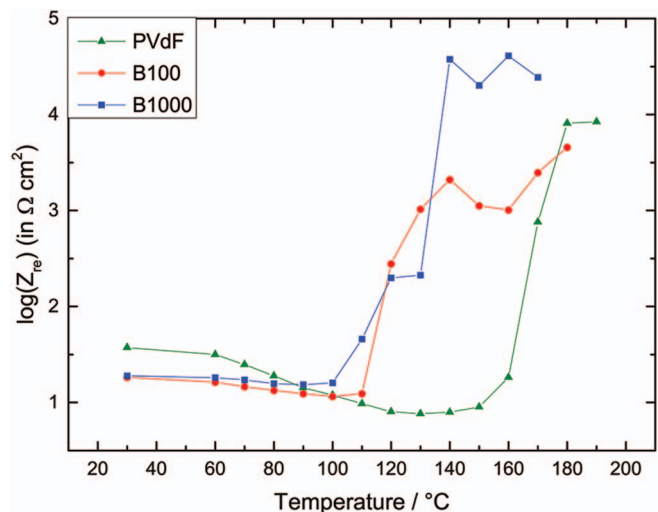
For shutdown temperature, i.e. where the EPS starts to soften and close pores, $\log Z_{re}$ (at 1 kHz) was plotted vs. temperature (Figure 8). Although PEO has great affinity with liquid electrolyte and Li ion can move through the melted PEO regions, the B100 curve clearly

Table II. Resistivity and MacMullin number of tested membranes at 30°C. The resistivity of LP30 electrolyte used for the MacMullin number calculation is also reported.

	Thickness (μm)	Resistivity (ohm cm)	MacMullin number
LP30 ³⁰	-	$8.25 \cdot 10^1$	1
PVdF	80	$6.59 \cdot 10^2$	8
B100	60	$8.70 \cdot 10^2$	10
B100p	50	$9.51 \cdot 10^2$	11
B1000	70	$5.42 \cdot 10^2$	6
B1000p	30	$7.81 \cdot 10^2$	9
Celgard2400 ^{43,44}	25		16

**Figure 7.** Nyquist plots of PVdF, B100 and B1000 separators at 30°C, soaked in LP30 electrolyte. In the inset a magnification of high frequency values.

indicates that shutdown starts at 110°C and ends at about 140°C, the Z_{re} value having increased by two orders of magnitude. By contrast, B1000's shutdown process occurs between 100°C and 140°C, with resistance growing by three orders of magnitude. The interval of both blends are in line with the ideal shutdown temperature, which was set at 135°C for a conventional separator and at $100 \pm 10^\circ\text{C}$ for an advanced separator by the United States Advanced Battery Consortium (USABC).⁴⁵ A shutdown temperature of 160°C like that of

**Figure 6.** (a) Pristine B1000 separator (left) vs. pressed B1000p separator (right), SEM images of (b) PVdFp, (c) B100p and (d) B1000p membranes.**Figure 8.** Logarithm of Z_{re} , at 1 kHz vs. temperature over shutdown tests of electrolyte-soaked EPSs.

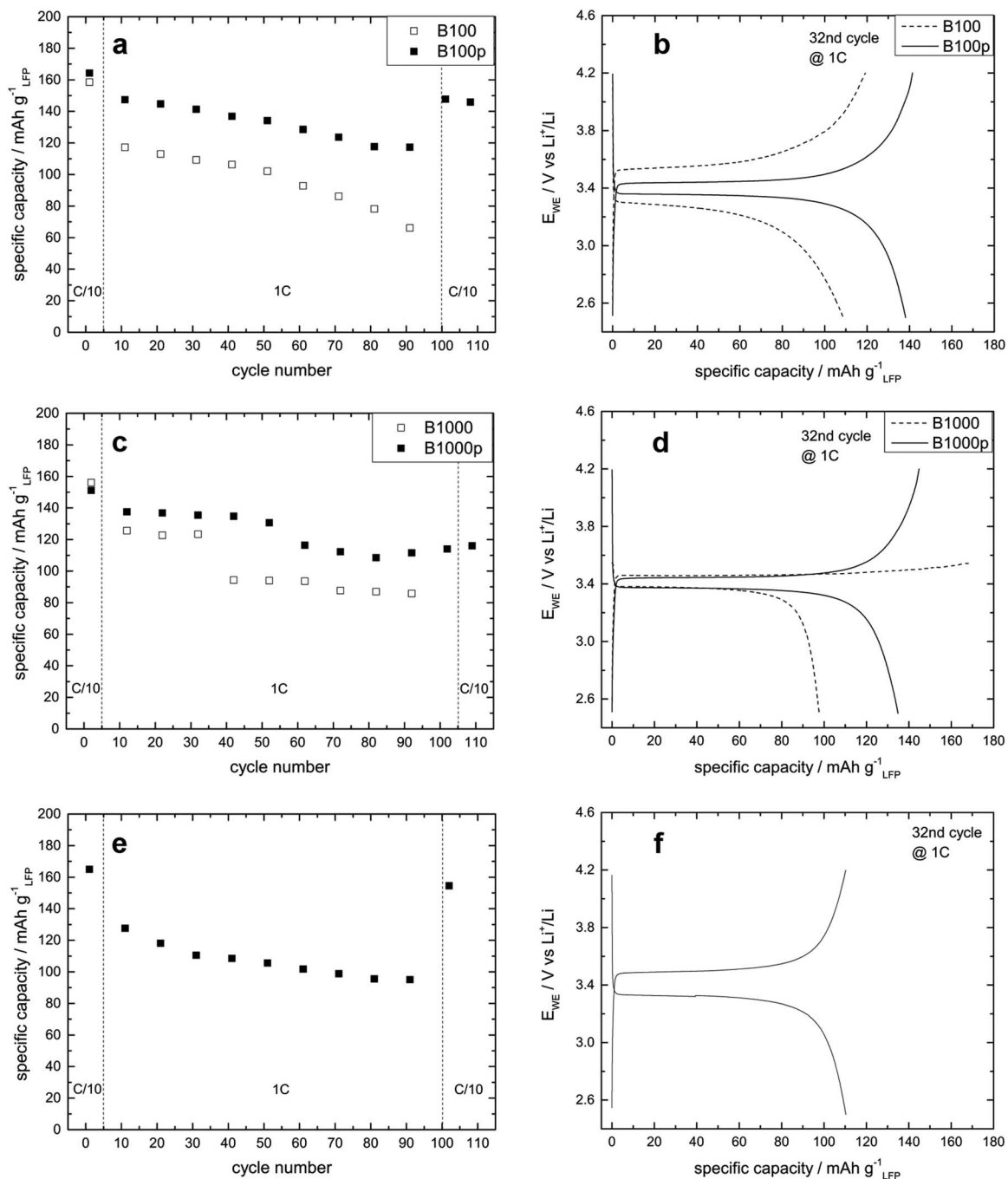


Figure 9. Galvanostatic charge/discharge cycles of Li/LiFePO₄ at 30°C in 3-electrodes mode between 2.5 V and 4.2 V vs. Li⁺/Li in LP30. Stability test at 1C with initial and final cycles at C/10 and potential profiles of the 32nd cycle of half-cells with a-b) B100 and B100p, c-d) B1000 and B1000p, e-f) Celgard.

Celgard2400⁴⁴ or in the range 160–180°C like that of PVdF is too high, inducing pores occlusion when thermal runaway has already started. Hence, the blend of PEO and PVdF leads to an improvement in terms of safety. PEO content in the blend is low enough and the fibrous morphology of the membrane, which exhibits very high tortuosity, is suitable to guarantee shutdown properties. PEO lower melting temperature, which is about 60°–70°C, causes a shift of the shutdown temperature to lower values, making the separator safer. Hence, the material design proposed in this work, i.e. blending two polymers with significantly different melting points, represents a good approach to achieve the same shutdown performance of the widely used Celgard trilayer polypropylene/polyethylene/polypropylene.^{46–49} PEO, the low-melting polymer, is responsible for the shutdown func-

tion, while PVdF, the high-melting polymer, assures the mechanical integrity of the separator up to its melting point.⁵⁰

Electrochemical tests were performed in half-cell configuration Li/EPS/LiFePO₄ with a metal Li reference electrode between 2.5 and 4.2 V vs. Li⁺/Li. LiFePO₄ performance with the LP30-soaked EPS was investigated through deep galvanostatic charge/discharge cycles at 30°C. The first five cycles were carried out at C/10 to let the system settle down. A stability protocol consisting of 100 cycles at 1C was then run. The discharge capacity of the LiFePO₄ electrodes, coupled with B100 and B100p (pressed) separators, is shown in Figure 9a as a function of cycle number. Figure 9b shows the potential profiles of the 32nd cycle of the cells with the two separators. While a significant and fast capacity fade occurs when the B100 separator is used, the

performance of the LiFePO_4 electrode is improved with the B100p membrane, even in terms of overpotentials. Although the capacity fading is less evident in the half-cells assembled with B1000 and B1000p (Figure 9c) and the overpotentials seem similar (Figure 9d), the cell with B1000p does not recover the initial capacity after 100 cycles, as shown by the last cycle at C/10. Figure 9d also displays a lower coulombic efficiency of the half-cell with B1000. The coulombic efficiency of the galvanostatic charge and discharge cycles was near 100% for the first 30–40 cycles of the half-cells with both B100 and B1000 separators (pressed or not pressed) and then decreased to value lower than 50%. Similar values are reported by Hu et al.,⁵¹ who used a graft copolymer based on poly(oxoethylene) metacrylate-poly(dimethyl siloxane) as polymer electrolyte in the $\text{Li}/\text{LiFePO}_4$ half-cell. They found a higher discharge capacity decrease over 50 cycles at room temperature than that of our half-cells, and a similar decrease of coulombic efficiency, down to 50%, at 120°C. Such a low coulombic efficiency indicates that concurrent and unwanted reactions occur in the cell.

The cycling stability of the half-cell $\text{Li}/\text{Celgard2400}/\text{LiFePO}_4$ and the voltage profile of the 32nd cycle were also reported for comparison in the Figures 9e and 9f. Although the stability over repeated charge/discharge cycles was lower than that of half-cell with the blended PVdF-PEO separators, the coulombic efficiency was higher (98–99%) and nearly constant.

Given the high reactivity of Li, the use of half-cell with the Li counter electrode complicates the system. Indeed, the deposition/stripping of lithium during charge and discharge processes causes the development of dendrites, and the strongly reducing environment produces SEI on Li electrode and reactive species in the electrolyte medium. In this case, although EPSs are vulnerable to dendrites because of their high open porosity and low mechanical strength, dendrites do not seem to be the main problem. Reactive species produced on the electrode surface may retro-diffuse through the highly porous separator and react on the opposite electrode. This may also explain the better discharge capacity values of cells with B100p than of cells with B100, a result do as much to its reduced thickness as to a lower porosity that can hinder the shuttle movement of side-products. The chemical stability of EC, DMC and LiPF_6 , which are the three components of LP30, has a key-role in Li-ion battery performance. In particular LiPF_6 , whose reactivity is notably affected by the water and impurity content of the cell environment, may produce HF that can react with cell active and inactive components.^{52,53} The electrospun separator containing PEO, which is more hydrophilic than PVdF or polyolefines, may release water that triggers unwanted reactions in the presence of LiPF_6 . However, we found that the water content of the PVdF-PEO membranes is very low and does not change the water amount (ca. 20 ppm) in LP30 where the membranes were placed, as evaluated by KF coulometry.

After having excluded the presence of water in PVdF-PEO separators, we carried out tests on symmetrical Li/Li cells to evaluate if the reactivity observed in half-cells with these membranes were due to a higher impurity content in PVdF-PEO separators than in Celgard. Figure 10a displays the Nyquist plots of EIS measurements of the Li/Li cells after 0 and 56 hours in open circuit and Figure 10b the SEI resistance (R_{SEI}) evaluated from the fitting of the high frequency semicircle of the spectra over time. The high resistance values found for the B100, B1000 and Celgard separators are consistent with the building of SEI layers on Li electrodes held in open circuit for long times. The results of Li/Li cells with pressed separators displayed a high variability depending on their morphology, i.e. on the non-uniform porosity after pressing, as shown in Figure 6. The SEI layers built in presence of B100, B1000 and Celgard are very similar even in a high-reactivity environment like that in presence of Li metal, thus demonstrating that PVdF-PEO separators do not contain more impurities or reactive moieties than Celgard. LiFePO_4 is usually selected for its safe potential, and the conventional electrolyte is electrochemically stable at potential <4.2 V. However, the high reactivity at the LiFePO_4 surface was also evidenced by the fact that impedance spectroscopy in 3-electrode mode gave no good, reproducible spectra until a thick, stable and

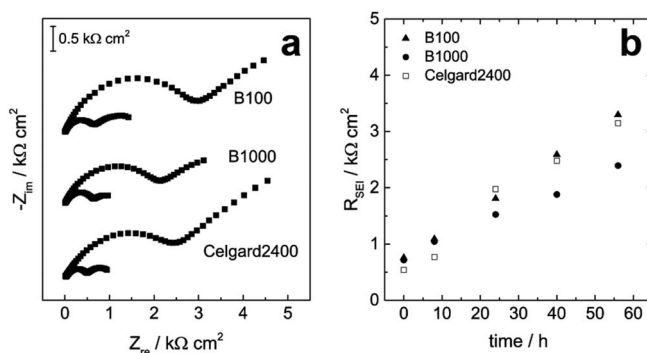


Figure 10. Li/Li cells with B100, B1000 and Celgard at 30°C in LP30 electrolyte: a) Nyquist plots at $t = 0$ and $t = 56$ hours and b) R_{SEI} over time.

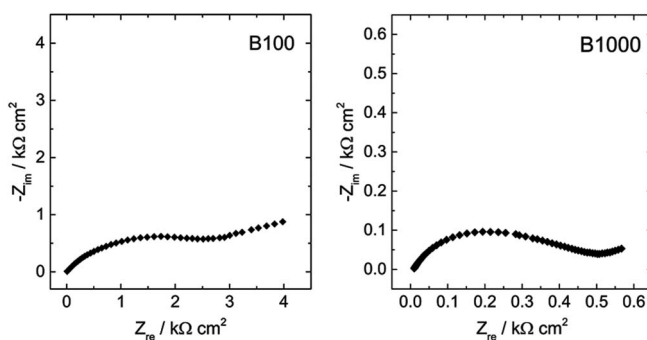


Figure 11. Nyquist plots of the charged LiFePO_4 electrode in half-cell with B100 and B1000 separators after 100 galvanostatic charge/discharge cycles at 30°C in LP30 electrolyte.

highly resistive surface was produced. Figure 11 shows the spectra of LiFePO_4 electrode recorded at the end of 100 cycles. Stability tests like those reported in Figure 9 for $\text{Li}/\text{LiFePO}_4$ half-cells were also performed on symmetric cells $\text{LiFePO}_4/\text{B100}/\text{LiFePO}_4$ with the counter electrode in great excess and the results are shown in Figure 12. The use of a symmetric cell enhances readings even if a decrease of coulombic efficiency from 99.5% to 97% occurs after 50 cycles. The capacity fade has to be ascribed not to a degradation of the material but to the difficulty in releasing the charge, i.e. in reinserting the Li^+ ion, during discharge at high rate; the discharge at low C-rate, indeed,

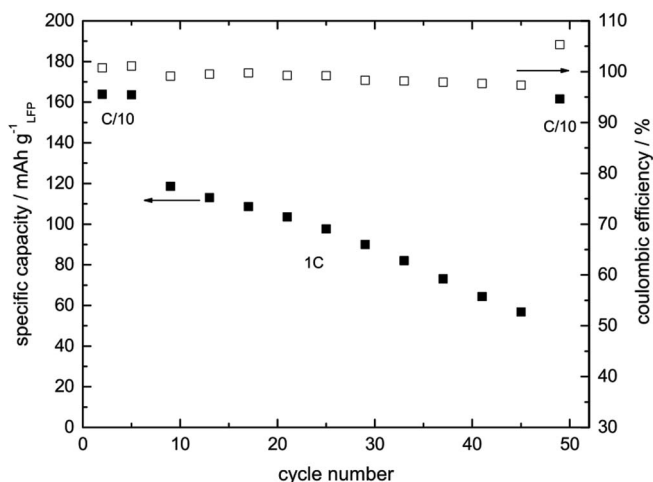


Figure 12. Galvanostatic charge/discharge cycles at 30°C at 1C with initial and final cycles at C/10 of a symmetric $\text{LiFePO}_4/\text{B100}/\text{LiFePO}_4$ in 3-electrode mode between 2.5 V and 4.2 V.

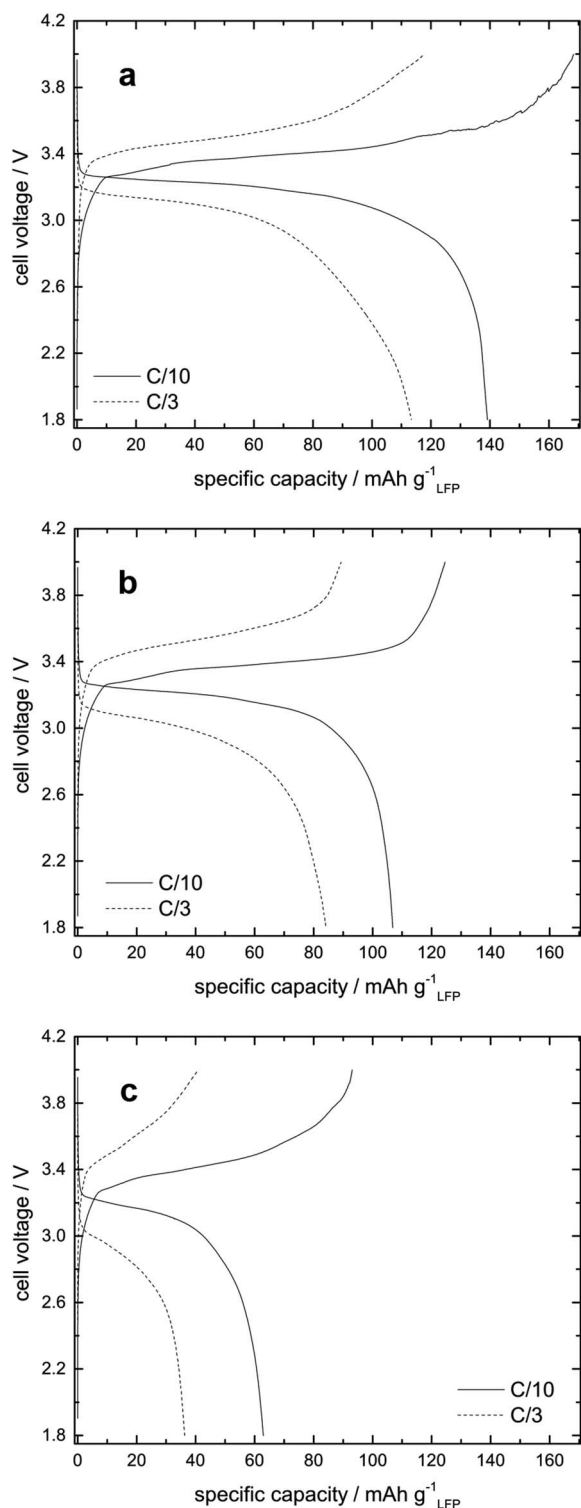


Figure 13. Galvanostatic charge/discharge cycles (2nd cycle at C/10 and 2nd cycle at C/3) of graphite/LiFePO₄ at 30°C in 2-electrode mode between 1.8 V and 4.0 V with different separators: a) B100p, b) B1000p and c) Celgard.

restores the initial capacity. These findings suggest that LP30 could be the main source of highly reactive species.

We then assembled full cells with LiFePO₄ positive electrode and graphite negative electrode to demonstrate the effectiveness of these EPSs as Li-ion battery separator. Electrode mass balancing was effected by setting the ratio of the capacity of the negative to that of the positive near 1.8, taking into account a practical capacity of

270 mAh g⁻¹ for graphite and of 150 mAh g⁻¹ for LiFePO₄ evaluated at 1C. Deep galvanostatic charge/discharge cycles were performed at 30°C in 2-electrode mode between 1.8 V and 4.0 V and applying C/10 and C/3 currents. Figure 13 shows the voltage profiles of the 2nd cycle at C/10 and the 2nd cycle at C/3 of the full cells with B100p and B1000p as separators. The charge/discharge voltage profiles of the full cell with Celgard separator are also given for comparison. The cells with electrospun PVdF-PEO separators display better performance than those with Celgard both in terms of specific capacity and of coulombic efficiency thus demonstrating that these membranes can be used in Li-ion cells.

Conclusions

New electrospun separators based on PVdF and PEO blends were yielded with good morphology and suitable thickness. Their properties as separators are convincing, with great electrolyte uptake, low MacMullin number and lower shutdown temperature than those of PVdF and polyolefine tested for comparison. Their mechanical properties are comparable to those of pure PVdF but sub-par compared to those of polyolefins. It was observed that the electrochemical stability of electrospun separators improves after pressing. This suggests that membrane porosity should not be too high to avoid both mixing of chemical species deriving from local side reactions, and possible growth of dendrites. We excluded water and impurity as the main cause of the reactivity of PVdF-PEO based separators and demonstrated in preliminary studies that the use of such electrospun membranes in Li-ion cells is feasible.

Acknowledgments

This research was done thanks to the financial support of Italian Ministry of Research and University (MIUR) and of the PLASMAT project (Alma Mater Studiorum - Università di Bologna FARB grant for fundamental research). Support of the COST Action MP1206: "Electrospun nanofibres for bio inspired composite materials and innovative industrial applications" is also acknowledged.

References

1. C. Barchasz, F. Molton, C. Duboc, J.-C. Leprêtre, S. Patoux, and F. Alloin, *Anal. Chem.*, **84**(9), 3973 (2012).
2. A. Fotouhi, D. J. Auger, K. Proppa, S. Longoa, and M. Wild, *Renewable Sustainable Energy Rev.*, **56**, 1008 (2016).
3. C. Liu, F. Li, L.-P. Ma, and H.-M. Cheng, *Adv. Mater.*, **22**, E28 (2010).
4. B. Melot and J.-M. Tarascon, *Acc. Chem. Res.*, **46**(5), 1226 (2013).
5. B. Scrosati and J. Garche, *J. Power Sources*, **195**, 2419 (2010).
6. B. Scrosati, *J. Solid State Electrochem.*, **15**, 1623 (2011).
7. J. B. Goodenough and K.-S. Park, *J. Am. Chem. Soc.*, **135**, 1167 (2013).
8. B. Dunn, H. Kamath, and J.-M. Tarascon, *Science*, **334**, 928 (2011).
9. J. B. Goodenough and Y. Kim, *Chem. Mater.*, **22**, 587 (2010).
10. P. Arora and Z. Zhang, *Chem. Rev.*, **104**, 4419 (2004).
11. S. S. Zhang, *J. Power Sources*, **164**, 351 (2007).
12. X. Huang, *J. Solid State Electrochem.*, **15**, 649 (2011).
13. H. Lee, M. Yanilmaz, O. Toprakci, K. Fu, and X. Zhang, *Energy Environ. Sci.*, **7**, 3857 (2014).
14. P. G. Balakrishnan, R. Ramesh, and T. P. Kumar, *J. Power Sources*, **155**, 401 (2006).
15. C. J. Orendorff, *Electrochem. Soc. Interface*, **21**, 61 (2012).
16. J.-W. Jung, C.-L. Lee, S. Yu, and I.-D. Kim, *J. Mater. Chem. A*, **4**, 703 (2016).
17. S. Cavaliere, S. Subianto, I. Savych, D. J. Jones, and J. Rozière, *Energy Environ. Sci.*, **4**, 4761 (2011).
18. J. Nunes-Pereira, C. M. Costa, and S. Lanceros-Mendez, *J. Power Sources*, **281**, 378 (2015).
19. C. M. Costa, J. L. Gomez Ribelles, S. Lanceros-Méndez, G. B. Appetecchi, and B. Scrosati, *J. Power Sources*, **245**, 779 (2014).
20. S.-S. Choi, Y. S. Lee, C. W. Joo, S. G. Lee, J. K. Park, and K.-S. Han, *Electrochim. Acta*, **50**, 339 (2004).
21. K. Hwang, B. Kwon, and H. Byun, *J. Membr. Sci.*, **378**, 111 (2011).
22. Y. Ding, P. Zhang, Z. Long, Y. Jiang, F. Xu, and W. Di, *Sci. Technol. Adv. Mater.*, **9**, 015005 (2008).
23. Y. M. Lee, N.-S. Choi, J. A. Lee, W.-H. Seol, K.-Y. Cho, H.-Y. Jung, J.-W. Kim, and J.-K. Park, *J. Power Sources*, **146**, 431 (2005).
24. S. W. Lee, S. W. Choi, S. M. Jo, B. D. Chin, D. Y. Kim, K. Y. Lee, and J.-K. Park, *J. Power Sources*, **163**, 41 (2006).

25. F. Croce, M. L. Focarete, J. Hassoun, I. Meschini, and B. Scrosati, *Energy Environ. Sci.*, **4**, 921 (2011).
26. P. Martins, A. C. Lopes, and S. Lanceros-Mendez, *Prog. Polym. Sci.*, **39**, 683 (2014).
27. R. Prasanth, N. Shubha, H. H. Hng, and M. Srinivasan, *J. Power Sources*, **245**, 283 (2014).
28. W. Li, Y. Wu, J. Wang, D. Huang, L. Chen, and G. Yang, *Eur. Polym. J.*, **67**, 365 (2015).
29. L. S. Dolci, S. D. Quiroga, M. Gherardi, R. Laurita, A. Liguori, P. Sanibondi, A. Fiorani, L. Calzà, V. Colombo, and M. L. Focarete, *Plasma Processes Polym.*, **11**, 203 (2014).
30. M. Schmidt, U. Heider, A. Kuehner, R. Oesten, M. Jungnitz, N. Ignat'ev, and P. Sartori, *J. Power Sources*, **97**, 557 (2001).
31. R. Khajavi and M. Abbasipour, in *Electrospun Nanofibers*, M. Afshari, Editor, p.109, Woodhead Publishing, Duxford, (2017)
32. S. L. Shenoy, W. D. Bates, H. L. Frisch, and G. E. Wnek, *Polymer*, **46**, 3372 (2005).
33. M. Zaccaria, D. Fabiani, G. Cannucciari, C. Gualandi, M. L. Focarete, C. Arbizzani, F. De Giorgio, and M. Mastragostino, *J. Electrochem. Soc.*, **162**(6), A915 (2015).
34. J. Zheng, A. He, J. Li, and C. C. Han, *Macromol. Rapid Commun.*, **28**, 2159 (2007).
35. W.-W. Cui, D.-Y. Tang, and Z.-L. Gong, *J. Power Sources*, **223**, 206 (2013).
36. B. Mohammadi, A. A. Yousefi, and S. M. Bellah, *Polym. Test.*, **26**, 42 (2007).
37. G. Botelho, S. Lanceros-Mendez, A. M. Gonçalves, V. Sencadas, and J. G. Rocha, *J. Non-Cryst. Solids*, **354**, 72 (2008).
38. M. Richard-Lacroix and C. Pellerin, *Macromol.*, **48**, 4511 (2015).
39. A. Koski, K. Yim, and S. Shivkumar, *Materials Letters*, **58**, 493 (2004).
40. K. Gao, X. Hu, C. Dai, and T. Yi, *J. Mater. Sci. Eng. B*, **131**, 100 (2006).
41. H. Li, Y.-M. Chen, X.-T. Ma, J.-L. Shi, B.-K. Zhu, and L.-P. Zhu, *J. Membr. Sci.*, **379**, 397 (2011).
42. R. Laurita, M. Zaccaria, M. Gherardi, D. Fabiani, A. Merlettini, A. Pollicino, M. L. Focarete, and V. Colombo, *Plasma Processes Polym.*, **13**, 124 (2016).
43. D. Djian, F. Alloin, S. Martinet, H. Lignier, and J. Y. Sanchez, *J. Power Sources*, **172**, 416 (2007).
44. C. Arbizzani, F. Colò, F. De Giorgio, M. Guidotti, M. Mastragostino, F. Alloin, M. Bolloli, Y. Molméret, and J.-Y. Sanchez, *J. Power Sources*, **246**, 299 (2014).
45. USABC Lithium Battery Separator Goals, http://www.uscar.org/guest/article_view.php?articles_id=85, Last accessed July 2016.
46. R. M. Spotnitz, US Pat. 6,180, 280 (2001).
47. H. Higuchi, K. Matsushita, M. Ezoe, and T. Shinomura, US Pat. 5,385,777 (1995).
48. E. P. Roth, D. H. Doughty, and D. L. Pile, *J. Power Sources*, **174**, 579 (2007).
49. C. L. Cheng, C. C. Wan, Y. Y. Wang, and M. S. Wu, *J. Power Sources*, **144**, 238 (2005).
50. A. La Monaca, Separatori polimerici elettrofilati per batterie Li-ione, *MSc Degree Thesis*, University of Bologna (2016).
51. Q. Hu, S. Osswald, R. Daniel, Y. Zhu, S. Wesel, L. Ortiz, and D. R. Sadoway, *J. Power Sources*, **196**, 5604 (2011).
52. D. Aurbach, M. Moshkovich, Y. Cohen, and A. Schechter, *Langmuir*, **15**, 2947 (1999).
53. S. Wiemers-Meyer, S. Jeremias, M. Winter, and S. Nowak, *Electrochim. Acta*, **222**, 1267 (2016).